COSMIC RAY ANISOTROPIES OBSERVED LATE IN THE DECAY PHASE OF SOLAR FLARE EVENTS

F. R. ALLUM, R. A. R. PALMEIRA*, K. G. McCRACKEN**, and U. R. RAO‡
The University of Texas at Dallas, P.O. Box 688, Richardson, Tex. 75080, U.S.A.

D. H. FAIRFIELD
Goddard Space Flight Center, Greenbelt, Md. 20771, U.S.A.

and

L. J. GLEESON‡‡
University of California, San Diego, La Jolla, Calif. 92037, U.S.A.

(Received 12 September, 1973, in revised form 10 June, 1974)

Abstract. Concurrent interplanetary magnetic field and 0.7–7.6 MeV proton cosmic-ray anisotropy data obtained from instrumentation on Explorers 34 and 41 are examined for five cosmic-ray events in which we observe a persistent eastern-anisotropy phase late in the event ($t \gtrsim 4$ days). The direction of the anisotropy at such times shows remarkable invariance with respect to the direction of the magnetic field (which generally varies throughout the event) and it is also independent of particle species (electrons and protons) and particle speed over the range $0.06 \leqslant \beta \leqslant 0.56$. The anisotropy is from the direction $38.3° \pm 2.4°$ E of the solar radius vector, and is inferred to be orthogonal to the long term, mean interplanetary field direction. Both the amplitude of the anisotropy and the decay time constant show a strong dependence on the magnetic field azimuth. Detailed comparison of the anisotropy and the magnetic field data shows that the simple model of convection plus diffusion parallel to the magnetic field is applicable for this phase of the flare effect.

It is demonstrated that contemporary theories do not predict the invariance of the direction as observed, even when the magnetic field is steady; these theories need extension to take into account the magnetic field direction ψ varying from its mean direction ψ_0. It is shown that the late phase anisotropy vector is not expected to be everywhere perpendicular to the mean magnetic field. The suggestion that we are observing kinks in the magnetic field moving radially outwards from the Sun leads to the conclusion that the parallel diffusion coefficient varies as $1/\cos^2(\psi - \psi_0)$. Density gradients in the late decay phase are estimated to be $\approx 700\%$/AU for 0.7–7.6 MeV protons. A simple theory reproduces the dependence of the decay time constant on anisotropy; it also leads to a radial density gradient of about 1000%/AU and diffusion coefficient of 1.3×10^{20} cm^2 s^{-1}.

1. Introduction

The broad characteristics of the anisotropies observed in solar cosmic-ray events have been established in previous analyses of data obtained by experiments on Pioneers 6–9 and Explorers 34 and 41. Most of these characteristics are discussed in the review of McCracken and Rao (1970).

In particular, direct comparison with the interplanetary magnetic field (McCracken

Permanent address:
* INPE, São José dos Campos, São Paulo, Brazil
** CSIRO, G.P.O., Box 136, North Ryde, N.S.W., Australia
‡ Indian Scientific Satellite Project, Peenya, Bangalore, India.
‡‡ Monash University, Clayton, Australia

Solar Physics **38** (1974) 227–256.

et al., 1968), and inference based on the azimuth of the cosmic-ray anisotropy observed at late times in a flare effect, (McCracken *et al.*, 1967, 1971; Rao *et al.*, 1971) has firmly established the role of both convection and diffusion in the expulsion of cosmic rays from the solar system. That is, it has been shown that at all times during a flare event the net cosmic-ray anisotropy vector $\boldsymbol{\delta}$ may be represented as the resultant of the anisotropy arising from the convective ($\boldsymbol{\delta}_c$) and the diffusive ($\boldsymbol{\delta}_d$) components, namely

$$\boldsymbol{\delta} = \boldsymbol{\delta}_c + \boldsymbol{\delta}_d . \tag{1}$$

The component $\boldsymbol{\delta}_c$ is parallel to the plasma velocity, and the component $\boldsymbol{\delta}_d$ is parallel to the interplanetary magnetic field **B**. As the relative importance of these two components varies throughout the duration of a solar flare event, the observed temporal variation of the anisotropy shows distinct phases characteristic of each component as one or the other dominates the propagation process.

In recent papers it was shown that the cosmic-ray anisotropy for protons at very late times is directed from $\simeq 45°$E of the radial direction in the 0.7–45 MeV kinetic energy range (McCracken *et al.*, 1971; Rao *et al.*, 1971). Concurrent interplanetary magnetic field data were not available at the time, and an untested hypothesis was advanced that the anisotropy at late times was normal to the interplanetary magnetic field.

Several theoretical investigations have been made (Axford, 1969; Ng and Gleeson, 1971a, b; Ng, 1972) producing models which reproduce the general characteristics of the anisotropy. However, these models in general predict that $\boldsymbol{\delta} \cdot \mathbf{B} \neq 0$ and furthermore that the direction of $\boldsymbol{\delta}$ in the late decay phase will be a function of energy. These models assumed the interplanetary magnetic field to be in the form of the average Archimedes spiral.

In the present paper the earlier work is extended by making direct comparison between simultaneous measurements of the cosmic-ray anisotropy and magnetic-field vectors during five solar flare events. In most cases the magnetic-field direction varies significantly through the event. Most emphasis is given to the analysis, in the kinetic energy range 0.7–7.6 MeV, of the late decay phase, particularly the dependence of the amplitude and direction of $\boldsymbol{\delta}$ on magnetic-field azimuth. The dependence of the decay-time constant on magnetic-field direction and the dependence of $\boldsymbol{\delta}$ on species and energe are also examined. Some of the implications of these results for theoretical models are examined.

The principal results are that in the late decay phase the direction of $\boldsymbol{\delta}$ is essentially invariant with respect to the direction of the magnetic field, particle energy, and species, and that the amplitude of $\boldsymbol{\delta}$ and the decay time constant are each strong functions of the direction of the magnetic field.

An investigation of the dependence of $\boldsymbol{\delta}$ on **B** has also been made by Innanen and Van Allen (1973) for protons in the kinetic energy range >0.3 MeV. That work complements the present study of the early part of the events but it was not extended into the late decay phase.

2. Observations

The particle data reported in this paper were obtained from the UTD cosmic-ray anisotropy detectors on Explorers 34 and 41. A full description of the instruments, energy channels available and the data handling procedures are given elsewhere (Bartley *et al.*, 1971). In this paper we restrict ourselves to data obtained from the solid-state detectors in the low-energy range, viz., 0.7–7.6 MeV. Briefly, the instrument axis is mounted perpendicular to the spin axis of the satellite, and consequently scans a great circle parallel to the ecliptic plane. The counting rate is obtained from eight, 45 degree sectors in this plane. The anisotropy amplitude and direction are determined by fitting a sinusoid of the form

$$A_0 + A_1 \cos(\phi - \phi_{cr}) \tag{2}$$

to the set of eight data points. The relative amplitude, after correcting for averaging effects, and the azimuthal direction of maximum intensity of the first harmonic are given by 1.026 (A_1/A_0) and ϕ_{cr} respectively.

The magnetic-field data were obtained by triaxial fluxgate magnetometers on the same spacecraft. The sensors were mounted on six-foot booms to minimize spacecraft fields and the sensors were rotated every 3.9 days to obtain accurate instrumental zero levels. The instruments operated in their most sensitive ranges in the interplanetary medium (± 32 gamma on Explorer 34 and ± 40 gamma on Explorer 41) and the eight-bit digitization produced uncertainties of ± 0.16 gamma and ± 0.20 gamma respectively. Vector measurements were obtained every 2.56 s. For additional instrumental details see Fairfield (1969) and Fairfield and Ness (1972).

In the experimental portion of this paper, we will use the following conventions. The cosmic-ray azimuth, ϕ_{cr}, is the direction in the ecliptic plane *from* which the maximum particle flux is observed and is measured positive west (W) of the Earth-Sun line so that a particle flux *from* 45° E of the radial direction is equivalent to $\phi_{cr} = 315°$. The magnetic-field azimuth, ϕ_m, gives the direction in the plane of the ecliptic in which the interplanetary magnetic field is pointing and is measured positive east (E) of the Earth-Sun line. If the maximum particle flux is observed from the direction in which the magnetic field is pointing, then $\phi_{cr} = 360° - \phi_m$. These definitions are those used independently by the cosmic-ray and magnetic-field experimenters in their previous publications.

In this study the events selected must be large enough to provide significant fluxes of solar cosmic rays >4 days after injection, this being the time required for the eastern anisotropy to develop. This restricts our attention to events which have long decay phases that are observable with the Explorer 34/41 detectors; they are generally, but not entirely, large events. The flare events that show the easterly anisotropy and which will be analyzed herein are listed in Table I. Also listed are the times for which useful information could be extracted from the data, namely 5, 7, 8, 10, and 15 days. Our experience indicates that the development of an easterly anisotropy in the energy range (0.7–7.6 MeV) is common pattern of behaviour. We in fact are of the opinion

TABLE I

Flare identifications and onset times

Date	Parent flare IMP – region coordinates	Time of onset of eastern anisotropy	ϕ_m		Duration of observations
			West	East	
1967					
10 Nov.	Not identified	From onset	Yes	No	10 days
16 Dec.	2B 9118 N 23 E 66	20 Dec., 0400 UT	Yes	Yes 20 Dec., 1800 UT 21 Dec., 1000 UT	5 days
1968					
18 Nov.	1B 9760 N 21 W 87	21 Nov., 0600 UT	Yes	No	8 days
3 Dec.	3N 9802 N 18 E 80	8 Dec., 0700 UT	Yes	Yes 8 Dec., 0700-1400 12 Dec., 0200-1500	15 days
1969					
25 Sept.	2N 10326 N 14 W 14	1 Oct., 0000 UT	Yes	No	7 days

that the development of an easterly anisotropy phase is the normal pattern of behaviour in the *late* decay phase of large solar particle events, but that in order to observe this phase the event must be followed for many days (perhaps ~ 10). Exceptions to this pattern certainly exist however and future investigations will attempt to further define the physical phenomena contributing in these cases.

3. The Inter-Relationship of δ and B

To illustrate the inter-relationship between the cosmic-ray anisotropy vector $\boldsymbol{\delta}$ and the magnetic-field vector **B**, Figures 1, 3, and 5 display the consecutive hourly averages (plotted vectorially) of $\boldsymbol{\delta}$ projected into the ecliptic plane for three of the events discussed herein. We also include, at approximately six hour intervals, the corresponding projection of the interplanetary-magnetic-field direction into the ecliptic plane. The three phases of the flare effect that have been recognized in earlier papers (McCracken *et al.*, 1971) are shown. These are:

(a) The early, field aligned, anisotropy phase, in which diffusion dominates, and $\boldsymbol{\delta}$ is approximately parallel to **B** (McCracken *et al.*, 1968); in this phase the cosmic-ray density gradient is negative.

(b) The radial anisotropy phase, in which the convective diffusion dominates; in this phase, the cosmic ray density gradient is approximately zero.

(c) The easterly anisotropy phase, in which diffusion is driving cosmic rays *towards* the Sun, i.e., the cosmic-ray density gradient is positive (McCracken and Rao, 1970; McCracken *et al.*, 1971; Rao *et al.*, 1971; Ng and Gleeson, 1971a, b).

In some of the previous papers these phases were referred to respectively as the

non-equilibrium, equilibrium (radial), and equilibrium (eastern), phases; these terms have been replaced by the above because, as our understanding has increased, we have found that they do not describe the phenomena adequately.

Inspection of Figures 1, 3 and 5 shows that the magnetic vector in the second and third phases makes large, and various, angles with the anisotropy vector $\boldsymbol{\delta}$. This will be examined more rigorously in what follows. We note also that during the easterly phase of the anisotropy there is usually only a minor perturbation of the anisotropy vector at the time of a change in the direction of **B**, and that the perturbation dies out

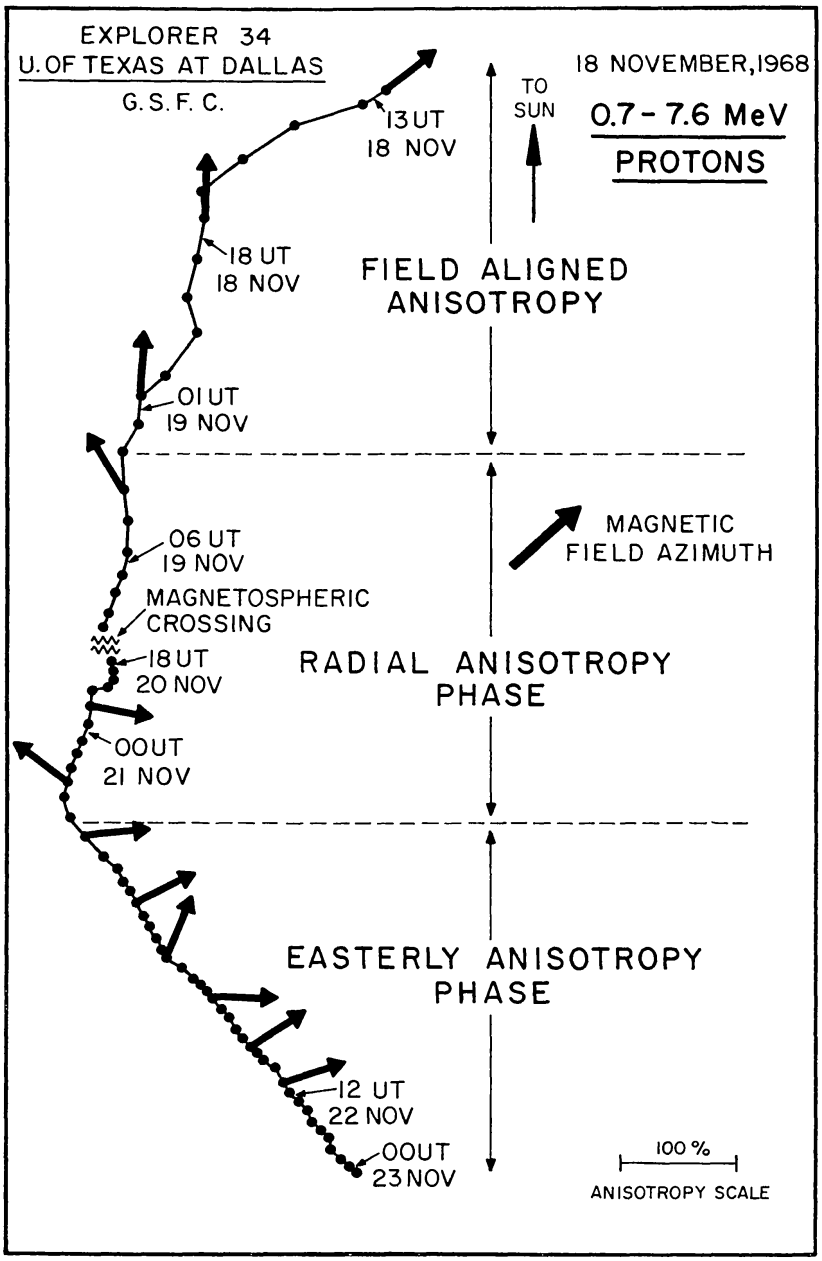

Fig. 1. The hourly anisotropy vector diagram for the flare event of November 18, 1968. The three distinct phases in the evolution of the anisotropy of a solar cosmic-ray event are indicated on the diagram. The hourly average direction of the magnetic field shown at approximately 6 hr intervals, is indicated also on the figure.

in several hours, δ reverting to the direction evident prior to the change of **B**. This temporal invariance of the direction of δ is established conclusively in the following.

Figures 2 and 4 present the time profiles for the events whose anisotropy diagrams are given in Figures 3 and 5. The periods during which the anisotropies exhibit the several phases are identified. As has been noted previously, the eastern phase of the anisotropy corresponds to the smoothly decaying portion of the flare effect. The events in Figures 2 and 4 are unusual in that the interplanetary field is from the east for prolonged periods of time, and this feature will be discussed in some detail in Appendix 1.

The anisotropy diagrams for all 5 events in Table I were used to identify the various phases of each of the flare events. After elimination of the periods of time in which the magnetometer and cosmic-ray anisotropy data gave evidence that the satellite was within the influence of the Earth's magnetic field, the following criteria were applied:

(a) The early, field aligned, anisotropy; data taken during the onset phase of the event, when the anisotropy amplitude is large ($>20\%$) and when $\phi_{cr} \geqslant 15°$ averaged over a period of time $\gtrsim 6$ hr.

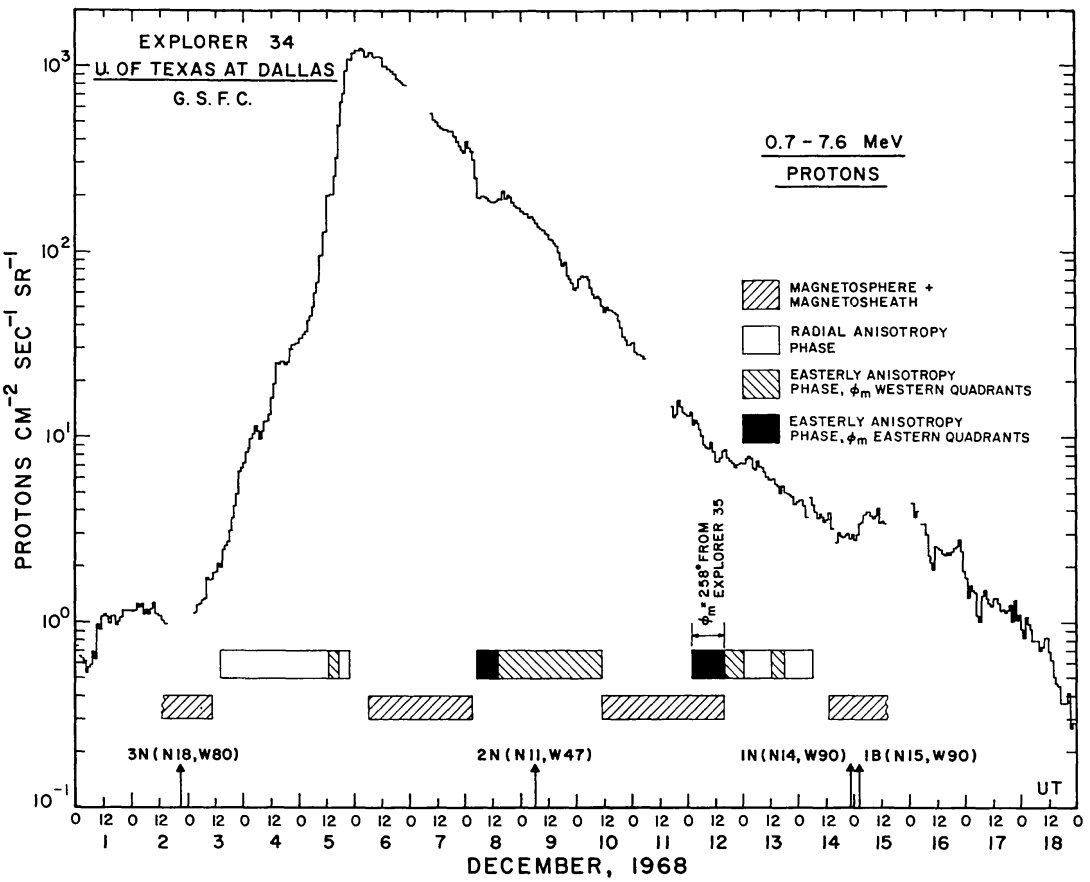

Fig. 2. The intensity-time profile of the low-energy protons following the 3F flare at 2116 UT, December 2, 1968. The times at which Explorer 34 crossed the magnetosheath and the magnetopause are indicated. We also show the intervals during which the characteristic anisotropy phases are observed, including those periods when the magnetic field is in the eastern quadrants during the eastern anisotropy phase.

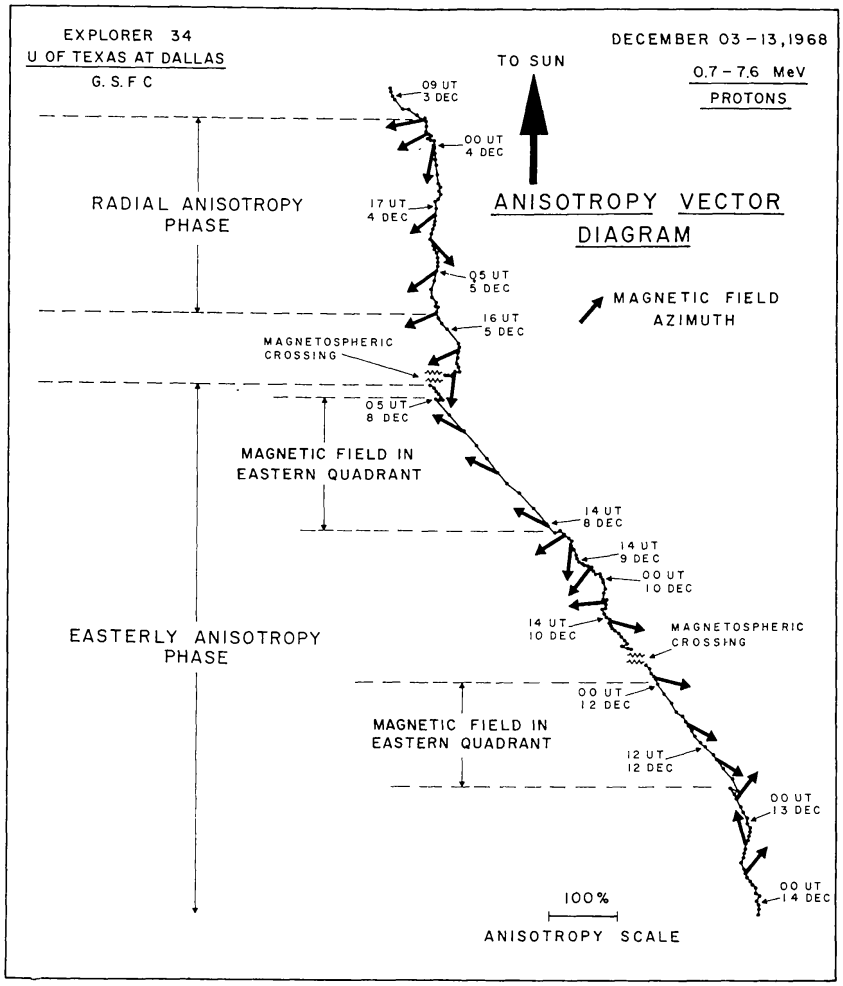

Fig. 3. The hourly anisotropy vector diagram for the flare event of December 3, 1968. The hourly average direction of the magnetic field shown at approx. 6 hr intervals is indicated also on the figure. The intervals during which Explorer 34 traversed the magnetosphere and magnetosheath are shown.

(b) The radial anisotropy; data taken after the field-aligned phase when the azimuth of the cosmic-ray anisotropy is within $\pm 15°$ of the radial direction, averaged over a a period of $\gtrsim 6$ hr.

(c) The easterly anisotropy; data taken following the development of the radial anisotropy. The azimuth of the cosmic-ray anisotropy must be consistently from the east for many hours (usually days) and $\phi_{cr} < 345°$ averaged over $\gtrsim 6$ hr periods.

The implementation of these criteria is demonstrated in Figures 1, 3 and 5. While the criteria affect the mean ϕ_{cr} within the class so chosen, they do not in any way restrict the range of ϕ_m that reports into each class, and hence the selection criteria will not bias the dependence of ϕ_m on ϕ_{cr} within each class.

The inter-relationship between the anisotropy and the magnetic field in each of the three phases defined above is now investigated. In doing so all of the data from the five events are combined so that the results are not unique to any one event, but to the class as a whole.

3.1. Field aligned phase

Figure 6 displays the dependence of ϕ_{cr} upon ϕ_m during this phase. It is clear that the anisotropy of the 0.7–7.6 MeV radiation is essentially field aligned during this phase. The small departure from alignment has been investigated in detail for 7.5–45 MeV observations by McCracken *et al.* (1968) and attributed to the presence of the radial convective component at all times in addition to the field aligned diffusive component. The solid curve is the dependence predicted in McCracken *et al.* (1968) when these two components are in the ratio 1:3.

These results, and the earlier results of McCracken *et al.* (1968), show that the anisotropy is essentially field aligned at early times throughout the whole energy range 0.7–45 MeV. This also establishes again that the diffusive component is always mainly field aligned, and thus that the parallel diffusion coefficient $\kappa_{\parallel}$ dominates over the perpendicular diffusion coefficient $(\kappa_{\perp}/\kappa_{\parallel} \ll 1)$.

We note that the data shown in Figure 6 are in contradiction to the results recently reported by Pyle (1973) who examined the anisotropy characteristics of low-energy protons (>0.66 MeV) from the University of Chicago experiment on Pioneer 7. Pyle concluded that, at these low energies, the particle flow, even in the early part of a flare event, was directed from approximately 30°E of the magnetic-field direction for almost every case that he had studied. From an examination of all of the data available to us from the UTD experiments on Explorers 34 and 41 (including data from events other than those shown in Figure 6) we must conclude that in the onset stages of a particle event, the low-energy proton anisotropy (0.7–7.6 MeV) is field aligned, as a

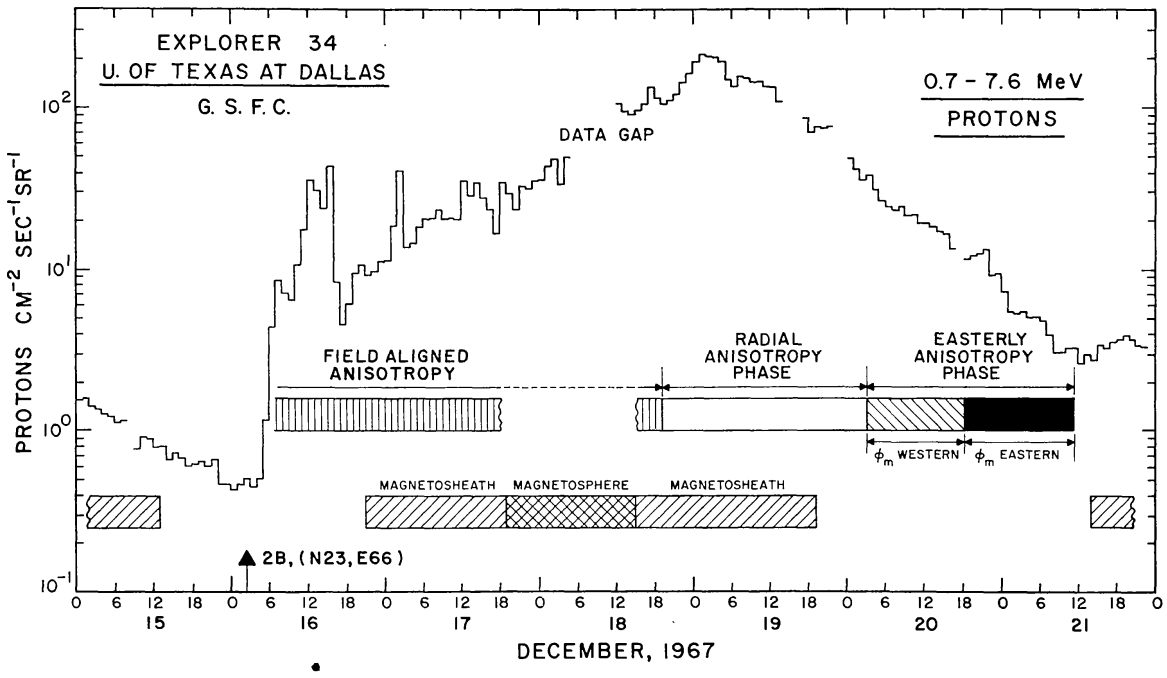

Fig. 4. The intensity-time profile for the flare event of December 16, 1967. The times of magnetosheath and magnetosphere crossing are indicated as well as the intervals during which the three different phases of the cosmic-ray anisotropy are observed.

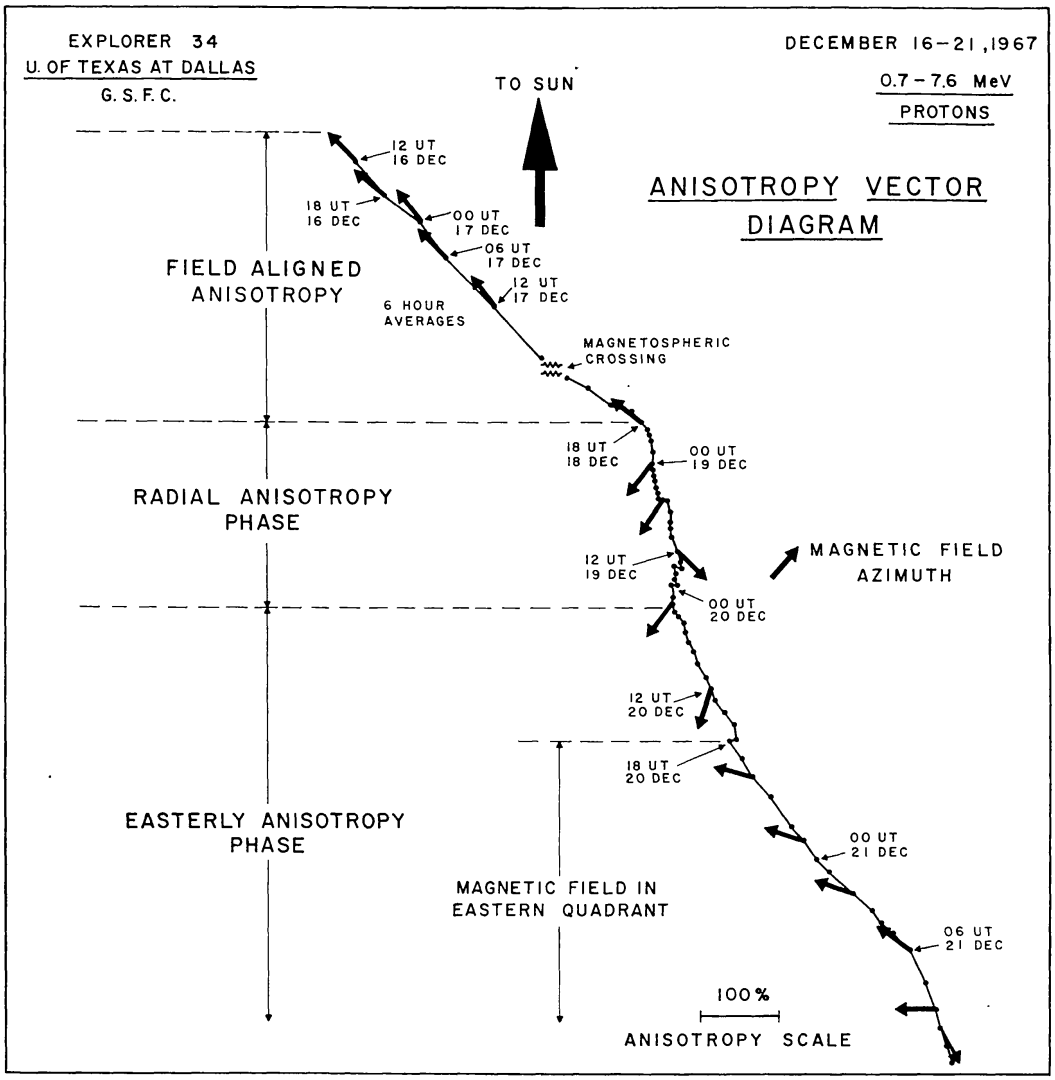

Fig. 5. The hourly average anisotropy vector diagram for the event of December 16, 1967. The prolonged early-phase anisotropy is clearly noticeable. For ease of presentation, the data prior to 1800 UT December 17, are shown as 6 hr averages. The hourly average direction of the magnetic field, shown at approx. 6 hr intervals, is indicated also on the figure. The times of magnetosheath and magnetospheric crossings are indicated also.

general rule, and that the case studied by Pyle must be considered as an exception to this general principle. A full discussion of our results and their relation to the analysis of Pyle are presented elsewhere (Rao *et al.*, 1973).

3.2. Radial anisotropy phase

Figure 7 shows ϕ_{cr} plotted against the magnetic field azimuth, ϕ_m, for the data set obtained during the radial phase of the five events. The fact that ϕ_m assumes a wide range of values during this phase of the flare event indicates that the development of a radial cosmic-ray flow is not sensitive to the contemporary direction of the interplanetary magnetic field.

Following McCracken *et al.* (1971) and earlier work noted therein, this phase has

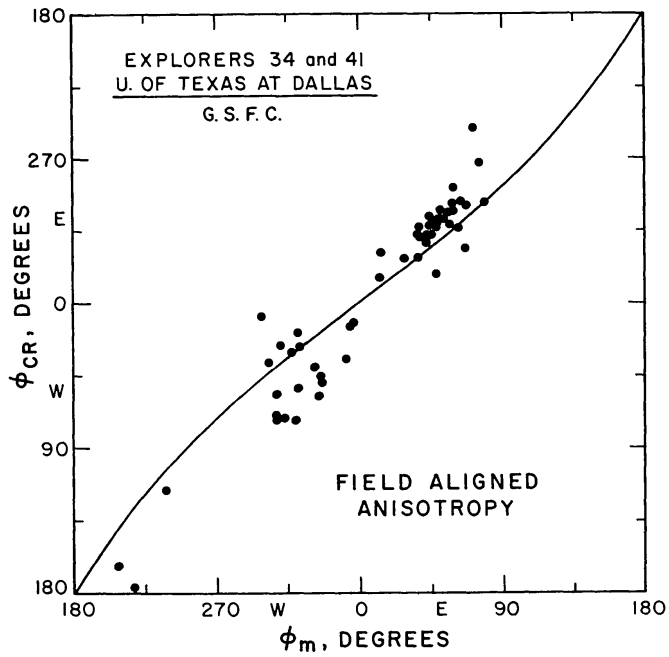

Fig. 6. The scatter diagram between the azimuth of the magnetic-field vector and the azimuth of the cosmic-ray anisotropy during the early phase of the five solar-flare events. The solid line shows a predicted relationship between ϕ_m and ϕ_{cr}, see text. Data points are 6 hr averages.

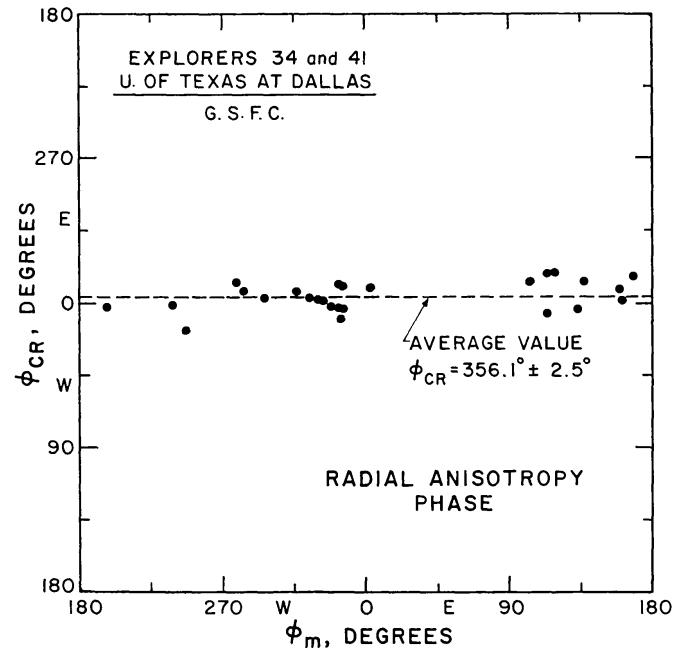

Fig. 7. The scatter diagram between the azimuth of the magnetic-field vector and the azimuth of the cosmic-ray anisotropy during the radial phase of the five solar-flare events. Data points are 6 hr averages.

been interpreted as occuring when the cosmic ray gradient is close to zero. At such a time, the particle flow will be entirely convective.

The average anisotropy amplitude for the data set displayed in Figure 7 is $9.8 \pm 1.0\%$. The theoretical convective anisotropy is radial with amplitude

$$\delta_c = 3CV/v = (2 + \alpha\gamma)V/v\,. \tag{3}$$

in which C is the Compton-Getting factor, $\alpha = 2$ (non-relativistic), V is the solar-wind speed, v is the mean particle speed, and γ is the kinetic-energy spectral index of the differential intensity j (Gleeson and Axford, 1969; Forman, 1970a, b). Our spectral data indicates γ averages 2 at late times in these events, hence representative values of the several parameters are taken as $\gamma = 2$; mean kinetic energy = 1.8 MeV; mean particle speed $v = 0.063c$; and $V = 390$ km s^{-1} (Wolfe, 1972). Using these we obtain $\delta_c = 12.4\%$ which is in reasonable correspondence with the observed value particularly when consideration is taken of the uncertainty in the spectral index γ and its influence on v.

This consistency, the independence of ϕ_m, and the earlier results of McCracken *et al.* (1968), confirm that the radial anisotropy is the result of convection alone throughout the entire kinetic-energy range 0.7–45 MeV.

3.3. Easterly-anisotropy phase

A total of 225 hr of data pertaining to the easterly anisotropy for the periods indicated in Table I have been grouped according to magnetic azimuth, ϕ_m, into 10° wide intervals (e.g., $\phi_m = 270°$–$280°$, $280°$–$290°$ . . $350°$–$360°$). Magnetic fields in opposite senses have been treated as identical for this purpose. The average amplitude, $\bar{\delta}_{cr}$ and azimuth, $\bar{\phi}_{cr}$, of the cosmic-ray anisotropy for each of these 10° intervals has been calculated as well as the average magnetic-field azimuth $\bar{\phi}_m$ for each interval (see Table II).

The mean cosmic-ray anisotropy vector for each interval of ϕ_m is shown in Figure 8 on a polar plot. The remarkable fact that is immediately evident is that as $\bar{\phi}_m$ varies

TABLE II

Magnetic-field azimuth and cosmic-ray anisotropies ($0.7 < T < 7.6$ MeV)

Range of ϕ_m degrees	$\bar{\phi}_m$ degrees	$\bar{\delta}_{cr}$ percent	ϕ_{cr} degrees	δ_d percent	δ_c percent
360–350	359.7	0.5 ± 0.5	319 ± 49		
350–340	345.8	3.4 ± 0.6	314 ± 14	10.0 ± 1.8	12.0 ± 2.1
340–330					
330–320	325.9	5.9 ± 1.1	314 ± 10	7.6 ± 1.4	10.4 ± 1.9
320–310	315.7	8.8 ± 2.1	326 ± 6	7.0 ± 1.7	12.3 ± 2.9
310–300	305.2	$9.9 + 1.6$	322 ± 4	7.5 ± 1.2	12.1 ± 2.0
300–290	294.9	10.6 ± 1.1	321 ± 4	7.4 ± 0.8	11.5 ± 1.2
290–280	285.3	13.8 ± 1.3	318 ± 3	9.6 ± 0.9	12.8 ± 1.2
280–270					
270–260	264.8	29.5 ± 2.8	326 ± 4	16.7 ± 1.6	23.0 ± 2.2
260–250	259.2	31.5 ± 3.5	322 ± 2	19.6 ± 2.2	21.3 ± 2.4

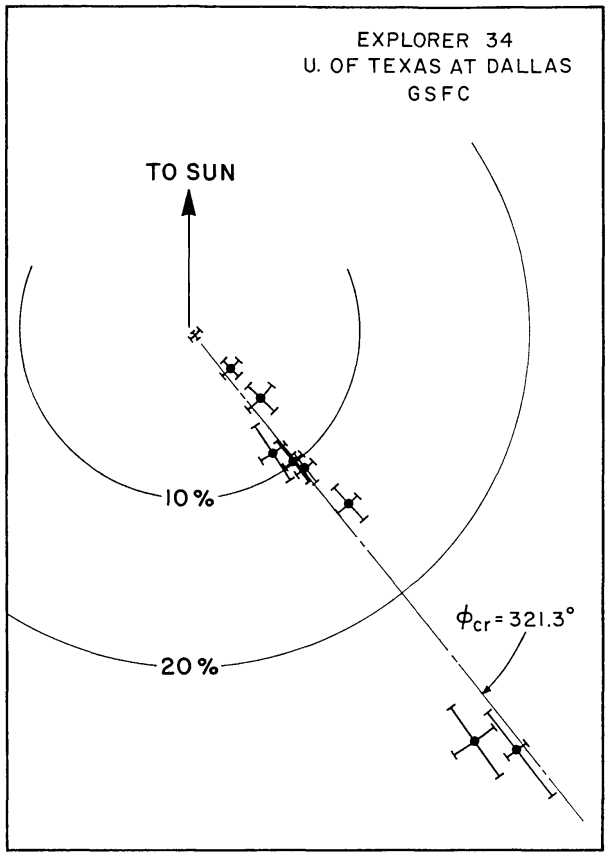

Fig. 8. The anisotropy vector $\boldsymbol{\delta}$ (i.e., amplitudes and azimuth), during the eastern-anisotropy phase, plotted on a polar diagram for the data presented in Table II. Even though the anisotropy amplitude changes by nearly two orders of magnitude, the azimuth is essentially invariant.

these vectors lie on a fixed line through the origin despite nearly two orders of magnitude change in the anisotropy amplitude, and a 100° change in magnetic vector direction. To show this independence more clearly, and that the result is not a consequence of the averaging process, we plot the individual ϕ_{cr} against ϕ_m in Figure 9. This figure again shows that ϕ_{cr} is constant and from these data we find the weighted mean azimuth for the population to be $\phi^*_{cr} = 321.3° \pm 2.4°$. The direction orthogonal to the observed invariant direction of $\boldsymbol{\delta}$ late in the solar flare event has a magnetic azimuth $\phi^*_m = 308.7° \pm 2.4°$ (as can be seen from the definition of ϕ_{cr} and ϕ_m illustrated in Figure 10).

The magnetic azimuth $\phi^*_m = 308.7 \pm 2.4$ is consistent with the long-term average azimuth of the interplanetary magnetic field. This is established by noting that the most probable solar-wind velocity of 390 km s^{-1}, given by Wolf (1972) for Explorer 34 and Heos 1 (1967 through 1969), implies an azimuth $\phi_m = 313°$; while the most probable value of the magnetic-field azimuth given by Ness (1970) is $\phi_m = 315° \pm 5°$. We conclude therefore that ϕ^*_{cr}, the invariant direction of the cosmic-ray anisotropy, is orthogonal, within prevailing statistical uncertainties, to the long-term average direction of the interplanetary magnetic field.

The cosmic-ray anisotropy in general consists primarily of a radial convective

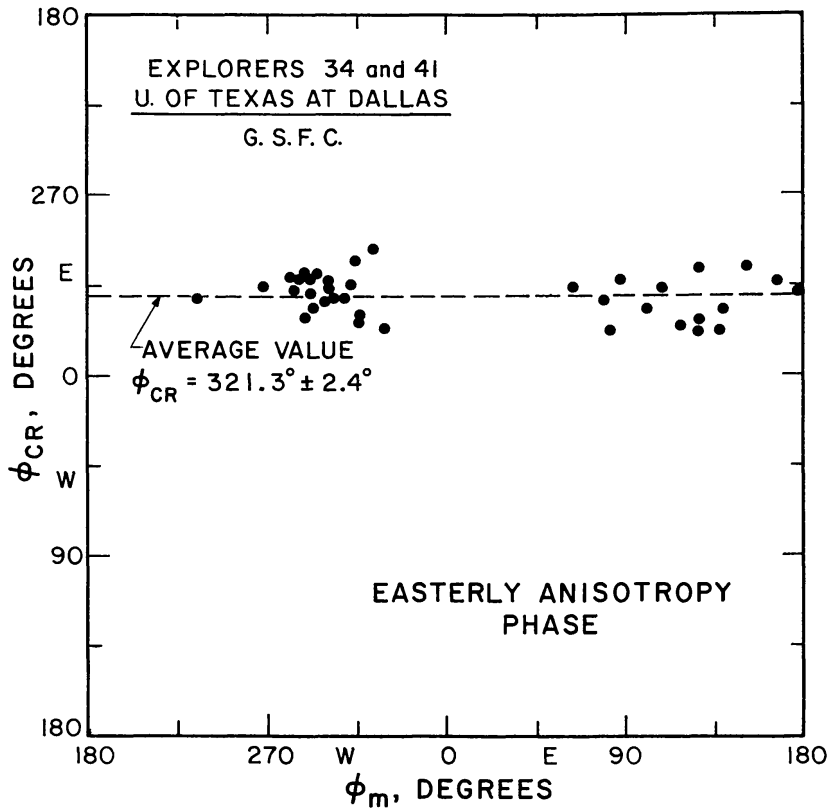

Fig. 9. The scatter diagram between the azimuth of the magnetic-field vector and the azimuth of the cosmic-ray anisotropy for the eastern-anisotropy phase of the five solar-flare events. The data points are 6 hr averages.

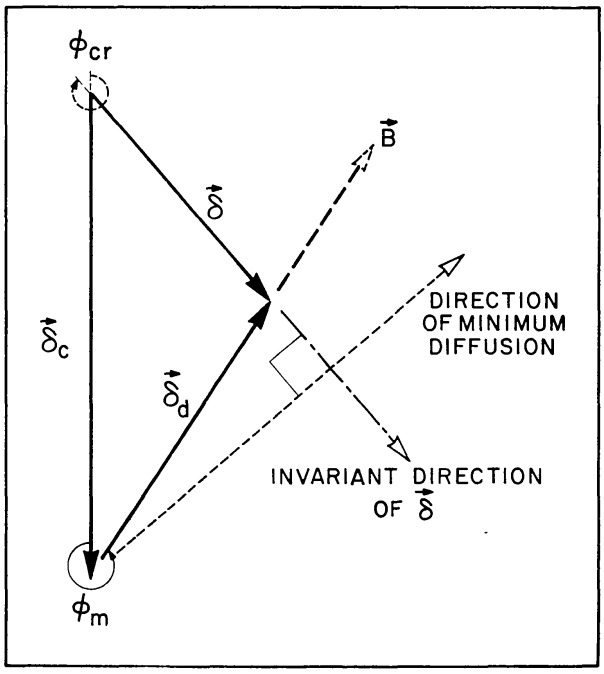

Fig. 10. Vector triangle representation of the eastern-anisotropy phase. The direction of the anisotropy remains invariant; the direction of the inward diffusion vector, δ_d, driven by the positive cosmic-ray gradient, is dependent on the direction of the local magnetic-field azimuth.

component δ_c and a diffusive component δ_d with

$$\boldsymbol{\delta} = \boldsymbol{\delta}_c + \boldsymbol{\delta}_d . \tag{4}$$

Assuming the diffusive component is field aligned, then $\boldsymbol{\delta}_d$ is in the direction of the magnetic field **B** and the vector triangle of components shown in Figures 10 applies. From it, the amplitudes δ_c, δ_d and δ are related by

$$\delta_c = \frac{\delta \sin(\phi_{cr} + \phi_m)}{\sin \phi_m}, \quad \delta_d = \frac{\delta \sin \phi_{cr}}{\sin \phi_m}. \tag{5}$$

From the above we may take $\phi_{cr} = \phi^*_{cr}$ and invariant.

The amplitudes δ_c and δ_d obtained from (5), using the observed mean values of δ, ϕ_{cr} and ϕ_m, are listed in Table II and plotted against ϕ_m in Figure 11. The derived convective anisotropies in Figure 11 for $270° < \phi_m < 350°$ are statistically identical.

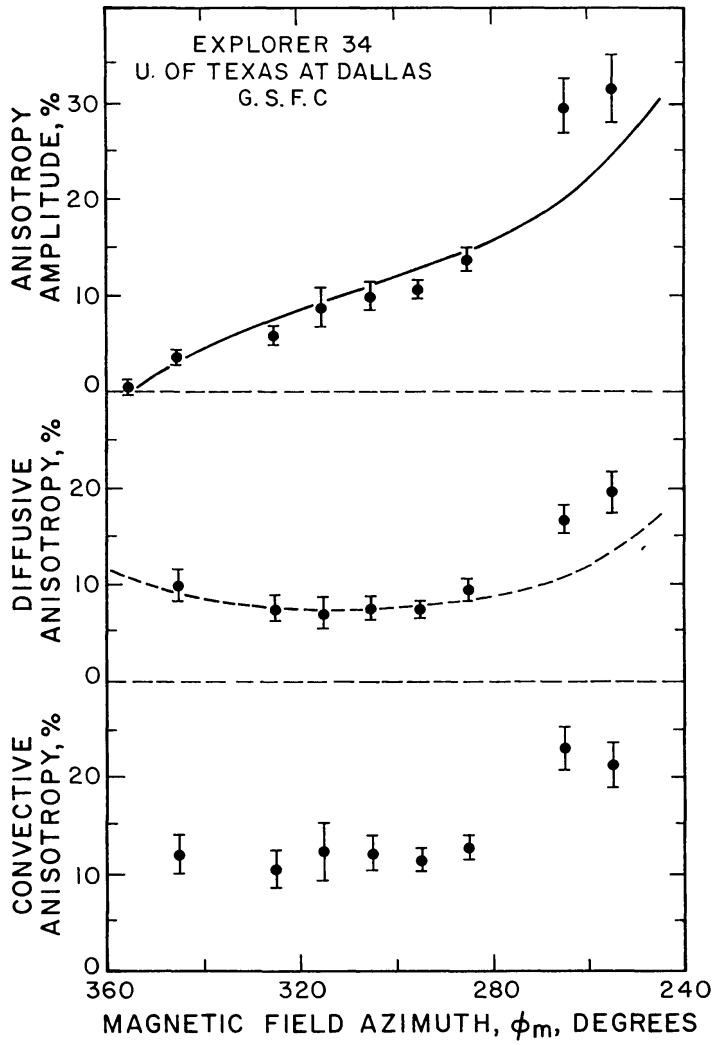

Fig. 11. The anisotropy amplitudes during the eastern-anisotropy phase plotted as a function of the interplanetary-magnetic-field azimuth. The lower set represents the convective component, the center set the diffusive component, and the upper set represents the total amplitude δ. The solid curves are derived from Equation (6) taking $\delta_c = 11.9\%$ and $\phi^*_{cr} = 321°$; see text.

Noting again the spectral and solar-wind dependence of δ_c [cf. Equation (3)], this suggests an essentially invariant solar-wind and spectral index γ. The weighted mean convective anisotropy for these data is $11.9 \pm 0.7\%$. This is very close to the theoretical convective anisotropy of 12.4% for these events deduced in the last subsection and identical to the observed value for the radial phase ($9.8 \pm 1.0\%$) at the 2σ significance level.

The higher values of δ_c obtained for the two points on the right-hand side of Figure 11 may be due to a substantially increased solar-wind speed and/or an enhanced spectral index during these occasions [cf. Equation (3)]. Allowing this, the invariance of the computed values of δ_c for $270 < \phi_m < 360°$, despite a factor of 60 change in δ, strongly supports the initial assumption made here and elsewhere (McCracken *et al.*, 1971) that the diffusion is field aligned even at these late times in the flare event.

The anisotropy magnitudes δ, and the diffusive components δ_d calculated from (5) by using the observational data, are also shown in Figure 11 as a function of ϕ_m. They exhibit a definite dependence on ϕ_m with δ_d having a broad minimum in the vicinity of $\phi_m \simeq 310°$ which we identify with the mean direction of the interplanetary field. If ϕ_{cr} is constant with value $\phi_{cr}^* = (7\pi/2) - \phi_m^*$ as in Figure 10, δ_d and δ are then related to δ_c by

$$\delta_d = \frac{\delta_c \cos \phi_m^*}{\cos(\phi_m - \phi_m^*)}, \qquad \delta = -\frac{\delta_c \sin \phi_m}{\cos(\phi_m - \phi_m^*)}. \tag{6}$$

The anisotropies according to these formulae are shown in Figure 11 by the full curves on the assumption that $\delta_c = 11.9\%$ and $\phi_{cr}^* = 321°$. There is good agreement with the data except for the two right-hand points, this discrepancy again being accounted for by larger values of δ_c.

No mention has been made, so far, of the component of **B** normal to the ecliptic and given by $\mathbf{B} \sin \theta_m$. For the 225 hr of data used here the distribution of $|\theta_m|$ is: $0° < |\theta_m| \leqslant 10°$, 32.7%; $10° < |\theta_m| \leqslant 20°$, 34.6%; $20° < |\theta_m| \leqslant 30°$, 24.2%; $30° < |\theta_m| \leqslant 44°$, 8.5%. The present analysis is not influenced significantly by this component of **B**. However, this may not be the case for analyses based upon detectors with smaller opening angles.

3.4. The decay time constant

Equation (9) of McCracken *et al.* (1971) suggests that the decay time constant, τ, in the last stage of the flare varies as $(\delta \cos \phi_{cr})^{-1}$. Although shown to be not strictly correct (Ng and Gleeson, private communication) this relationship suggests a strong dependence of τ upon δ which might be established with these observations in which δ changes by a factor of ~ 60 as ϕ_m changes. We have therefore extended our analysis to determine the dependence of τ upon δ and ϕ_m.

The decay time constant has been determined graphically by fitting a straight line decay to the hourly mean intensities for each 6 hr interval considered in the preparation of Figure 9. The reciprocal of the decay time constant, so found, is plotted against δ in Figure 12, and τ against the azimuth of the interplanetary magnetic field in

Figure 13. In the latter, the data have been averaged in 10° ranges of ϕ_m prior to plotting, as in the preparation of Table II, et seq. There is a considerable scatter of points in these figures, but a strong dependence of τ upon δ is apparent with τ decreasing as δ increases.

Some of this scatter may be due to the effect discussed by McCracken *et al.* (1971) that the particles are constrained to remain in a corotating magnetic flux tube and thus, as they sweep past the spacecraft, an azimuthal gradient in cosmic-ray density modifies the decay rate observed at the spacecraft. To determine the trend of the correction due to this effect, the parent flare was identified and the spacecraft position relative to the centroid of the cosmic ray population was determined. The estimated direction in which this would correct the points in Figure 12 is indicated by the arrows. Corrections to the points without arrows cannot be estimated.

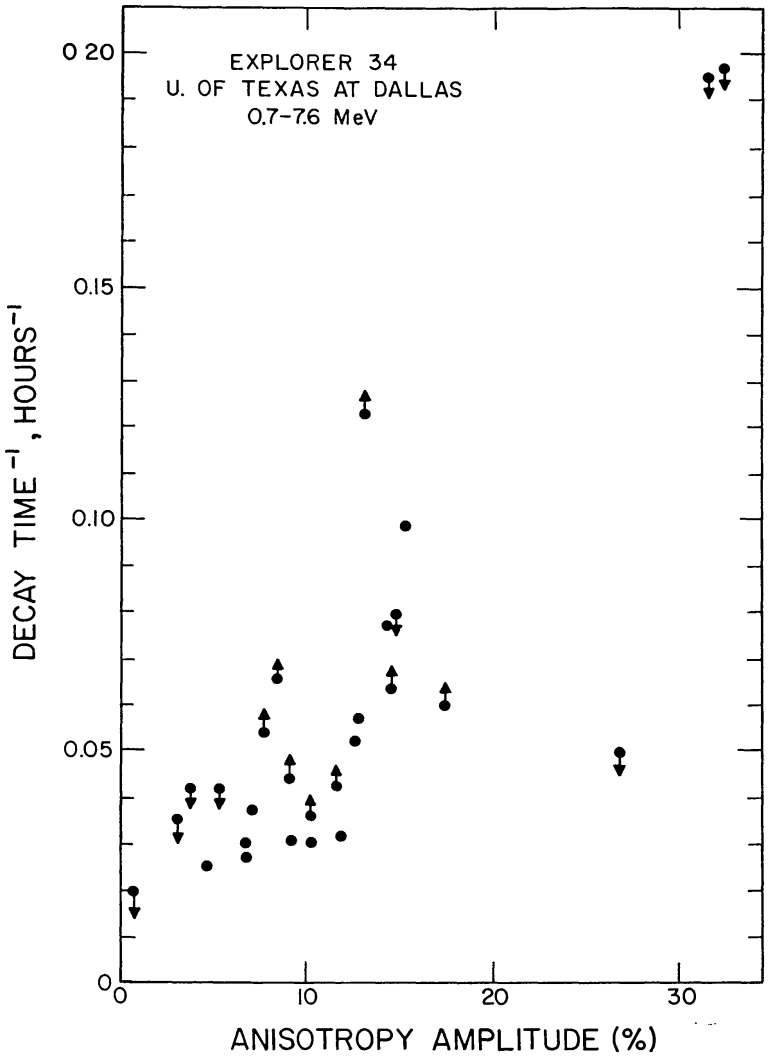

Fig. 12. The reciprocal of the decay time is plotted against the corresponding amplitude of the cosmic-ray anisotropy during the eastern-anisotropy phase for the 6-hr time intervals used in Figure 9. The arrows indicate the directions in which the data points would be moved if corrections were applied for the effect of an azimuthal gradient in the cosmic-ray density. The trend of the data suggests $1/\tau \sim \delta$.

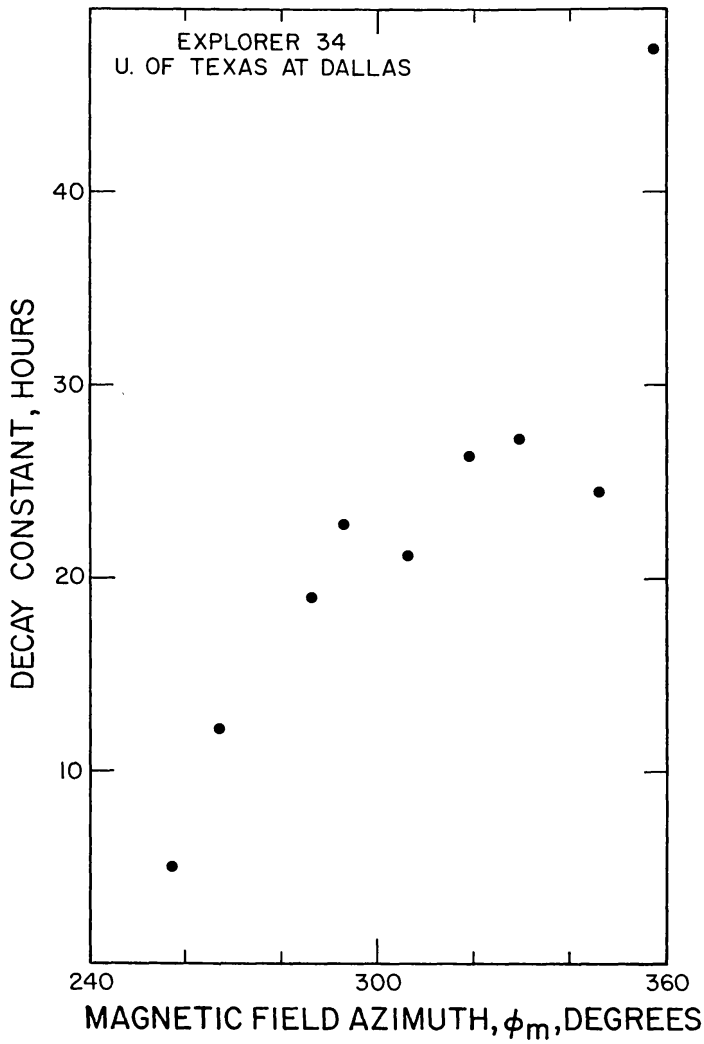

Fig. 13. The decay time constant is plotted as a function of the azimuth of the interplanetary magnetic field. As the magnetic field shows greater departure from the radial direction, $\phi_m = 360°$, the decay time constant decreases.

The azimuthal-gradient corrections probably reduce the scatter in Figure 12 and a linear fit through the points, determined by inspection is

$$1/\tau = 0.005 + 0.0055\ \delta \tag{7}$$

with τ in hours and δ in percent. This provides an empirical relationship between τ and δ (and hence ϕ_m) which we will discuss further under Theoretical Implications. Note that the relationship $\tau = 1.5\ r/v\delta \cos\phi_{cr}$ which was found by McCracken *et al.* (1971) to apply for radiation in the energy range 7.5–21.5 MeV, is not in good accord with the observations in the 0.7–7.6 MeV range, the time constants being consistently low compared with the estimate.

3.5. The dependence of the easterly phase on energy

In the preceding subsections we have examined in detail the dependence of the late-phase anisotropy and time decay constant on the magnetic-field azimuth for protons

of kinetic energy T in the interval 0.7–7.6 MeV having $\bar{\beta}$=(mean speed/speed of light) $\simeq$0.06. We now examine the data available at other energies.

We have reported previously the existence of long-lived eastern anisotropy phases for particles of higher velocity and of different species, viz., for protons with $7.5 \leqslant T \leqslant 21.5$ MeV, $\bar{\beta}=0.15$ (McCracken *et al.*, 1971), and for electrons with $T>70$ keV, $\bar{\beta}=0.56$ (Allum *et al.*, 1971). These investigations did not include a study of the concurrent interplanetary magnetic field. In Table III, and Figure 14, we summarize the dependence of ϕ_{cr} on particle speed and species using both the present and previously reported data for the eastern anisotropy phase.

It will be noted from Figure 14 that the anisotropy direction is essentially invariant for $0.06 \leqslant \bar{\beta} \leqslant 0.56$ and the mean for these observations, $\phi_{cr}=320.6°$, is statistically indistinguishable from the mean $321.3° \pm 2.4°$, derived from the data sample in Figure 8.

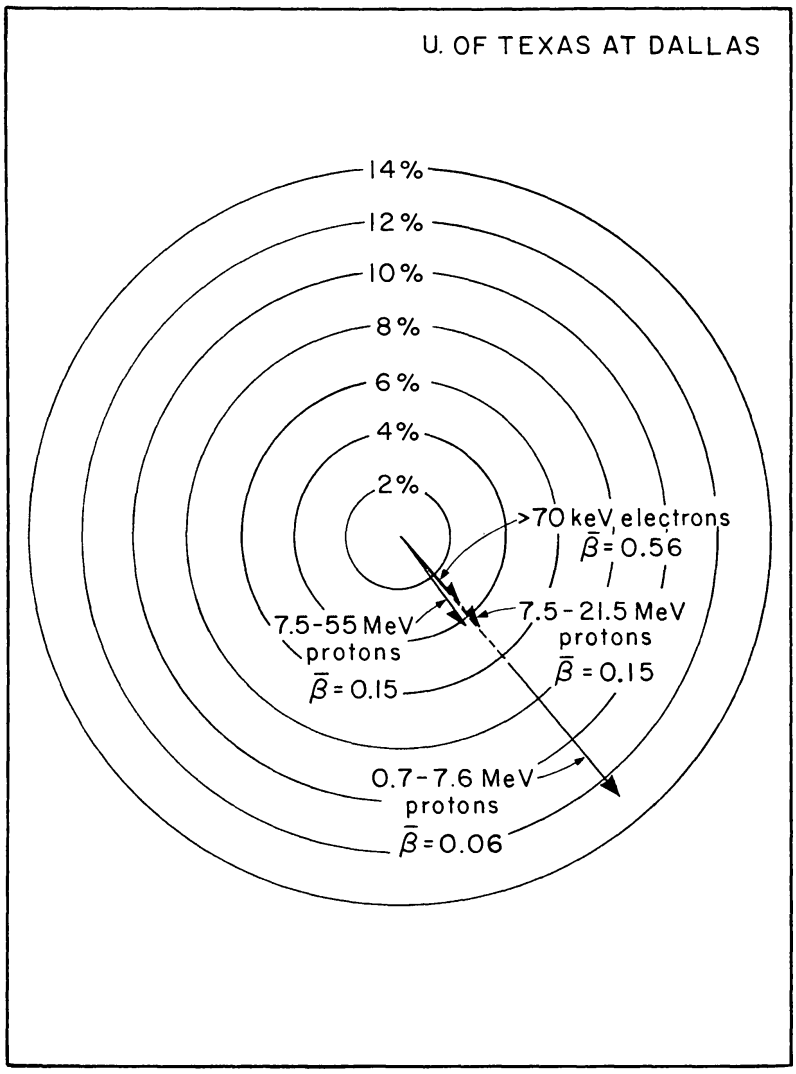

Fig. 14. The anisotropy amplitude and azimuth during the eastern-anisotropy phase plotted on a polar diagram for electrons and protons in three energy ranges. The anisotropy azimuth is invariant over the wide range of velocities, $0.06 < \bar{\beta} < 0.56$.

TABLE III

Data showing the dependence of δ' on species and kinetic energy

Particles	T MeV	$\bar{\beta}$	δ' percent	ϕ_{cr} degree	Source
Protons	0.7–7.6	0.06	12.6 ± 3.6	320.2 ± 1.5	Present paper; Table II, cols. 2 and 3
Protons	7.5–21.5	0.15	4.5 ± 0.6	319.4 ± 2.4	McCracken *et al.*, 1971; Table III, cols. 4 and 5
Protons	7.6–55	0.15	4.2 ± 0.7	323.7 ± 2.2	Rao *et al.*, 1971 Table III, cols. 7 and 8
Electrons	>0.07	0.56	3.3 ± 0.2	319 ± 4	Allum *et al.*, 1971; Table III, cols. 3 and 4

We conclude that the agreement between ϕ_{cr} in Figures 8 and 14 indicates that the phase of the easterly anisotropy is the same for all events and is invariant over a wide range of particle speed, $0.06 \leqslant \bar{\beta} \leqslant 0.56$. We also note that the work in this paper has shown that for protons with $\bar{\beta}=0.06$ the amplitude of δ is a strong function of the direction of the interplanetary magnetic field, ϕ_m. We expect this same pattern at other values of $\bar{\beta}$ and for other species and we also expect a dependence of the time decay constant on ϕ_m and δ.

If ϕ_m had remained at its mean value, 313°, for all the events, or if the sample sizes had been large, the constancy of ϕ_{cr} would require [cf. Equation (3) and Figure 10*f* that the anisotropy amplitudes in Figure 14 should be proportional to δ_c and hence inversely proportional to $\bar{\beta}$. They are not inversely proportional to $\bar{\beta}$ and we attribute this difference to the small samples and ϕ_m differing from its mean value.

4. Theoretical Implications

There are four major results of the observations which require consideration in the context of present models of solar-particle propagation, viz., (a) that the late-phase anisotropy near 1 AU is from $38.7° \pm 2.4°$ E for a wide range of particle velocities ($0.06 < \bar{\beta} < 0.56$), (b) that this direction is perpendicular to that of the mean magnetic field, (c) that the late-phase anisotropy vector remains constant in direction irrespective of the direction of the interplanetary magnetic field, and (d) the decay time constant and anisotropy amplitude are strongly dependent on the direction of the interplanetary magnetic field.

Note that the role of the subsequent discussions will be to demonstrate the implications of the above results in terms of contemporary theory. We will demonstrate in a quantitative manner the inability of the theory to adequately link together these, and other observational facts regarding the solar cosmic-ray expulsion process. We do not attempt to present a fully modified theory; we do seek, however, to define theoretical and experimental questions that are crucial for further advance in our understanding.

From the outset, here, we should recall that the theoretical studies of models re-

producing the three phases of the anisotropy and noted in the Introduction have in each case assumed that the interplanetary magnetic field is constant at each point in interplanetary space, and that it has the Archimedes spiral form predicted for average conditions. In contrast to this the present observations show **B** (averaged over 6 hr intervals) varies markedly through an event, so that these steady models are not complete in all the essential components and need extending. This extension to transient geometries may be difficult and we do not attempt it here, but rather indicate the essentials of such a model and make some deductions from the 'local' data obtained here.

It is fortunate that the *direction* of the late-phase anisotropy is invariant with respect to the magnetic field azimuth; because of this we can discuss the observed lack of energy dependence of this direction in the context of a steady normal magnetic-field pattern. We can use the present theoretical models and show some of their shortcomings. We do this first. Then we discuss extensions of the models to the transient geometry case and its effect upon the decay time constant.

In the following we distinguish quantities relating to mean magnetic-field conditions with the subscript zero: Thus, **B** is the interplanetary magnetic field, and $\mathbf{B}_0$ the mean value; **e** is an outward-directed unit vector parallel to **B**, and $\mathbf{e}_0$ is that parallel to $\mathbf{B}_0$; ψ is the angle between **e** and the Sun-spacecraft direction, and ψ_0 is the mean value; τ is the decay time constant, and τ_0 is the decay time constant when $\psi = \psi_0$. Note that in this section we change from the azimuth specifications ϕ_{cr}, ϕ_m, used in the observational work, and consistent with previous papers, to the more convenient ψ used in theoretical work.

4.1. The constant direction δ_m with energy

Predictions of the energy dependence of the late time anisotropy $\boldsymbol{\delta}'$ have been made by Ng and Gleeson (1971a, b) and Ng (1972). In their models the diffusive component was assumed to be parallel to the magnetic field so that **S**, the differential current density, or streaming, is given by

$$\mathbf{S} = C\mathbf{V}U - \kappa_{\parallel}\left(\frac{\partial U}{\partial \mathbf{r}}\right). \tag{8}$$

Here U is the differential number density, **V** is the solar-wind velocity, C is the Compton-Getting factor, $\kappa_{\parallel}$ is the parallel diffusion coefficient, and **r** is the position vector. The quantity measured in these observations is the anisotropy vector $\boldsymbol{\delta}$ related to **S** by $\boldsymbol{\delta} = 3\mathbf{S}/vU$; the terms on the right of (8) represent convection and parallel diffusion, respectively, and (4) also has these same two components.

With **S** specified by (8), Ng and Gleeson obtained solutions of the equation of transport for U, viz.

$$\frac{\partial U}{\partial t} + \frac{1}{r^2}\frac{\partial}{\partial r}(r^2 S_r) + \tfrac{1}{3}V\frac{\partial^2}{\partial r \partial T}(\alpha T U) = 0, \tag{9}$$

with r the heliocentric distance, t the time, S_r the radial component of **S**, and $\alpha = 2$

(non-relativistic). From these solutions S and δ were obtained. Such solutions reproduced the three phases of anisotropy observed in a solar flare event whether a free-escape boundary at finite heliocentric distance, or a diffusion region extending to infinity, was assumed.

As a specific, but representative, example of these model solutions we note that in the late-decay-phase in the case $\kappa_{\parallel} = \kappa_0 r/\cos^2 \psi_0$ and with U proportional to $T^{-\mu}$ the angle θ between the Sun-spacecraft line and the anisotropy vector is given by

$$\tan\theta = \left[\frac{V + \eta\kappa_0 - 2\kappa_0 - 2r/t}{2CV - (V + \eta\kappa_0 - 2\kappa_0 - 2r/t)}\right] \tan\Psi_0 \tag{10}$$

with

$$\eta = [(2 + V/\kappa_0)^2 + 8V(C-1)/\kappa_0]^{1/2}. \tag{11}$$

As $\kappa_0 \to \infty$ we have from Equation (10),

$$\tan\theta \to \left[\frac{2C - C(C-1)\,V/\kappa_0 - 2r/t}{C(C-1)\,V/\kappa_0 + 2r/t}\right] \tan\psi_0 . \tag{12}$$

This analytic solution is representative of many studied by numerical methods; it illustrates the swing of the anisotropy with time, predicts an increase in θ with diffusion coefficient (see below), and illustrates the spectral dependence, with θ decreasing as the spectrum steepens (μ increases).

From Equation (10), taking κ proportional to β (Wibberenz, 1971), taking $\kappa_{\parallel} = 5.4 \times 10^{20}$ cm^2 s^{-1} at $r = 1$ AU for 10 MeV protons, and with $C = 3$ and $V = 390$ km s^{-1}, we obtain θ' (the limiting value of θ at $t \to \infty$) as shown in Table IV for the three cases of different species and energy of interest here. With $C = 2$, the values of θ' increase and the range decreases to 20°; reducing $\kappa_{\parallel}$ by a factor of 2 decreases the θ' values but the ranges remain substantially the same. These values of θ', typically vary by about 25° in contrast to the observed invariance of $\pm 2.4°$. Hence, these predictions do not agree with the observations.

We conclude, therefore, that a major discrepancy between theory and experiment is provided by the invariance of the direction of δ with respect to energy, and that the ability to predict this invariance must be a crucial test of any theoretical models advanced in the future. We anticipate that this discrepancy will be resolved without changing the basic ideas in our theoretical work, but note that it may be that these and

TABLE IV

Assumed diffusion coefficients and derived θ' and G_r at $r = 1$ AU

Particles	β	κ_0 cm^2 s^{-1}	$\kappa_{\parallel}$ cm^2 s^{-1}	θ' degrees	G_r %/AU
> 70 keV electrons	0.56	7.0×10^7	2.1×10^{21}	71.0	100
7.5–21.5 MeV protons	0.15	1.9×10^7	5.6×10^{20}	53.4	300
0.7–7.6 MeV protons	0.06	7.3×10^6	2.2×10^{20}	41.9	700

other discrepancies discussed by Roelof and Krimigis (1973) will demand a fundamental revision.

4.2. The spatial dependence of $\boldsymbol{\delta}' \cdot \mathbf{B}_0$

The observations reported here (e.g., Figures 8, 14) have been made at $r = 1$ AU, and show that to a good approximation $\boldsymbol{\delta}'$, the late time anisotropy, satisfies $\boldsymbol{\delta}' \cdot \mathbf{B}_0 = 0$. The corresponding streaming, $\mathbf{S}'$, also satisfies $\mathbf{S}' \cdot \mathbf{B}_0 = 0$ near 1 AU. From this observation we are led to speculate that $\mathbf{S}' \cdot \mathbf{B}_0 = 0$ may be the case everywhere in interplanetary space. We shall now examine this possibility for $\mathbf{S}'_0$ the late-time streaming under average conditions and show that it leads to an inconsistency.

The method used is to assume that the property $\mathbf{S}'_0 \cdot \mathbf{B}_0 = 0$ is valid everywhere, and use this assumption, through the equation of transport (9) to deduce a relationship between the decay time constant, τ_0, and the radial gradient $G_r = (1/U)\, \partial U/\partial r$. We then check this relationship using the known value of τ and inferred values of G_r.

Assuming $\mathbf{S}'_0 \cdot \mathbf{B}_0 = 0$, and representing (8) by a vector triangle similar to Figure 10, we deduce $\mathbf{S}'_r = CVU \sin^2 \psi_0$. Substituting this into (9), noting that $\tan \psi_0 = \Omega r/V$ in the ecliptic plane (Ω = solar rotational velocity), and noting that $1/\tau = -(1/U)\, \partial U/\partial t$, we find

$$\frac{1}{\tau_0} = \frac{CV}{r}\,(4 \sin^2 \psi_0 - 2 \sin^4 \psi_0) + [C \sin^2 \psi_0 - (C-1)]\, VG_r \tag{13}$$

a relationship that must be satisfied if the assumption $\boldsymbol{\delta}' \cdot \mathbf{B}_0 \equiv 0$ is satisfied. Taking $r = 1$ AU, $C = 2.5$, $V = 390$ km s^{-1}, and in (AU)$^{-1}$ (13) becomes

$$\frac{1}{\tau_0} = \frac{1}{28} - \frac{G_r}{400}. \tag{14}$$

Note that the gradient enters into (13) and (14) from the conservation of particles term in (9) and also from the energy change term in that equation.

The gradient to be used in (14) can be obtained from (8) by noting that, in the late decay phase, the diffusion term S_d, is equal to $CVU \cos \psi_0$ (Figure 10) and, as earlier, adopting the diffusion coefficient reported by Wibberenz (1971). This yields $G_r \simeq 7$ (AU)$^{-1}$ for these 0.7–7.6 MeV particles and thus (14) predicts a decay time ≈ 53 hr. The observed valve of τ_0 under mean conditions reported herein is 20–25 hr (cf. Figures 12 and 13). The specific values which apply in (14) depend upon the value of C, and we find predicted values of τ_0 ranging from 38 hr with $C = 1$, to ~ 100 hr with $C = 3$. In each case the predicted τ_0 exceeds the observed value by a factor $\gtrsim 2$. On the basis of this inconsistency we conclude that the assumption $\boldsymbol{\delta}' \cdot \mathbf{B}_0 = 0$ everywhere is not valid.

It is relevant here to note the very high density gradients required to produce the late-phase anisotropy at $\theta' \approx 40°$. These gradients are listed in Table IV for the diffusion coefficients assumed. As noted above for 0.7–7.6 MeV particles, G_r is typically 700%/AU, and thus should be observable from radially separated spacecraft; its observation together with the anisotropies measured herein would provide a good

measure of the diffusion coefficient. We also note that in the only published case where a gradient has been measured during a long decay, it was found to be consistent with zero (Roelof and Krimigis, 1973; Roelof, 1973). However this event was not a simple one and the measurement was not made during the easterly anisotropy phase, so its relevance in the present context is not clear.

4.3. Invariance of the direction of the late time anisotropy

In Figure 8 we showed that the direction of the late-time anisotropy was independent of the concurrent direction of the interplanetary magnetic field, even when the magnetic field deviated some 70 deg from the nominal Archimedes spiral angle, ψ_0.

We suggest that in these periods we are observing magnetic-flux tubes which are distorted from the normal Archimedes spiral direction but still are being convected away from the Sun by the solar wind. Thus we envisage a 'kink' in the flux tube moving radially outwards with the sections of the tube on either side of the kink forming the normal Archimedes spiral. Figure 15 shows the kink at two times as seen from a fixed frame of reference. Typical dimensions of a kink may be 0.1–0.2 AU.

Our discussion will be made in terms of the bulk velocity $\mathbf{w}$ defined, in terms of the anisotropy $\boldsymbol{\delta}$, by

$$\mathbf{w} = (v/3C)\boldsymbol{\delta}\,. \tag{15}$$

The Compton-Getting factor, C, is included to take account of spectral effects; the velocity $\mathbf{w}$ is that with which an observer must move in order to see an isotropic distribution, i.e., zero anisotropy. As deduced previously (Equation (2)), the particles

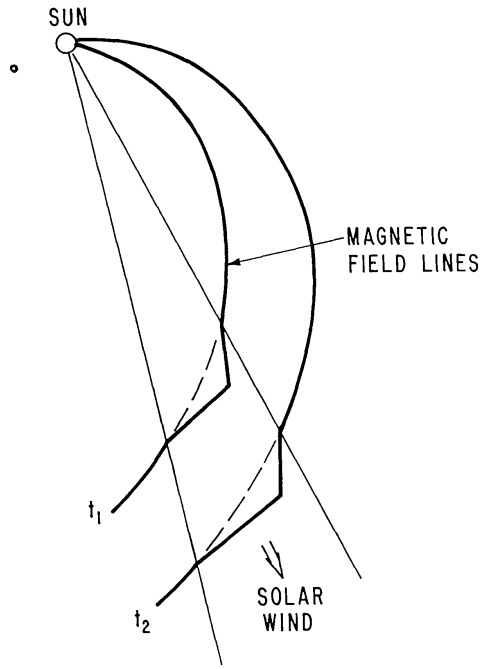

Fig. 15. Illustrating a kink in the magnetic field being carried out with the solar wind. The kink is shown for $r \sim 1$ AU and at times t_1 and t_2 separated by about 30 hr.

are considered to be constrained to stay within a magnetic flux tube so that

$$\mathbf{w} = \mathbf{V} + V_d\mathbf{e} \tag{16}$$

with $\mathbf{V}$ the solar-wind velocity and V_d the diffusive bulk flow speed, and $\mathbf{e}$, defined earlier, is the outward unit vector parallel to $\mathbf{B}$.

In the previous section we inferred from the data at $r=1$ AU that late in the decay phase $\boldsymbol{\delta}\cdot\mathbf{e}_0=0$, hence, now using $\mathbf{w}$ to represent the bulk velocity in this phase we have,

$$\mathbf{w}\cdot\mathbf{e}_0 = 0\,. \tag{17}$$

We now reinterpret this as showing that the component of $\mathbf{w}$, the bulk velocity, in the direction of the mean magnetic field remains as in the unperturbed case, even while the particles move within a kink. The additional bulk velocity, $\mathbf{w}-\mathbf{w}_0$, is perpendicular to $\mathbf{e}_0$ and simply allows the particles to move around the kink while maintaining the condition defined by (17).

We have already shown in the previous sub-section that we do not expect $\mathbf{w}_0$ to remain perpendicular to $\mathbf{e}_0$ at all heliocentric distances. Thus, Equation (17) must be replaced by something more general. We speculate that the principle will be that, at each heliocentric radius r, the component of the bulk velocity $\mathbf{w}$ in the direction $\mathbf{e}_0$ will remain constant. Written mathematically we expect

$$\mathbf{w}\cdot\mathbf{e}_0(r) = \mathbf{w}_0(r)\cdot\mathbf{e}_0(r) \tag{18}$$

for each $\mathbf{w}$ which, of course, is dependent upon the contemporary magnetic-field direction. The value of the right-hand side depends upon the heliocentric radius and our observations show that it has the value zero for $r=1$ AU. Equation (17) is now a special case of (4) appropriate at $r=1$ AU. If (18) is the constraining relationship the locus of $\mathbf{w}$ (or $\boldsymbol{\delta}'$) at $r\neq 1$ AU will still be a straight line perpendicular to $\mathbf{e}_0(r)$ but it will not in general retain a constant direction in space (Figure 16).

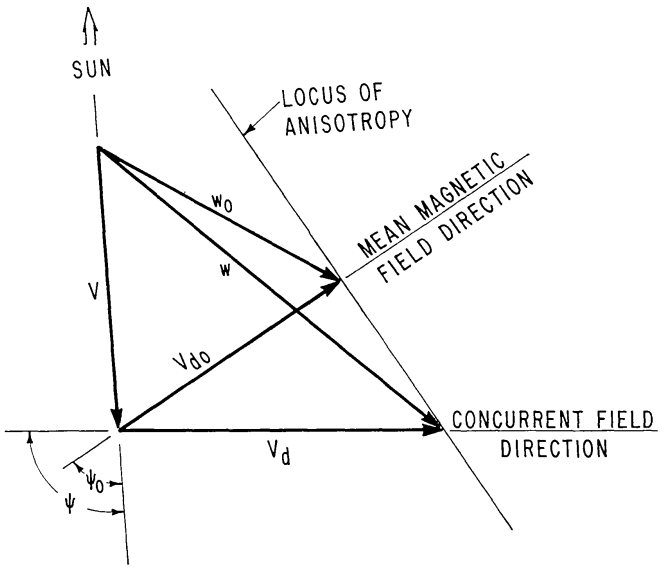

Fig. 16. Showing the form of the locus of anisotropy vectors suggested in the text at heliocentric distances other than 1 AU. The diagram is in terms of the bulk-velocity vectors and $\delta = 3Cw/v$.

The discussion so far has simply reinterpreted the observational result as an invariance of $\mathbf{w}\cdot\mathbf{e}_0$ at $r=1$ AU, and provided the hypothesis that this will be invariant at other heliocentric distances. We now deduce from this invariance some properties of the diffusion coefficient within the kink. Figure 17 illustrates the geometry assumed, and we compare cases when the flux tube is kinked and normal. The cross-section perpendicular to $\mathbf{e}_0$ is A, the volume considered is σ, the differential number density is U, and a distance measured along the flux tube is s. The corresponding quantities in the 'kink' are denoted by primes (A', U', σ', s') and we note that A' is taken to be perpendicular to $\mathbf{e}_0$.

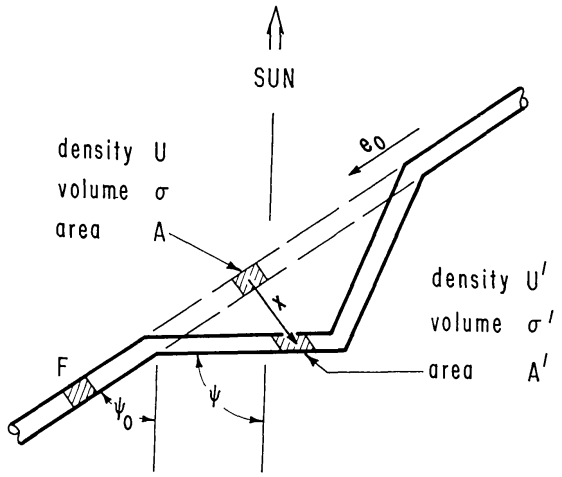

Fig. 17. Showing an idealized 'kink' together with an unperturbed magnetic-field flux tube, and corresponding volumes as inferred from $\mathbf{w}\cdot\mathbf{e}_0 =$ constant.

First we note that, since the bulk flow $\mathbf{e}_0$ is invariant, particles within the volume σ in undisturbed conditions will be found in the volume σ' under 'kink' conditions. Equating the number of particles we have

$$U'A'\,\mathrm{d}s'\cos(\psi-\psi_0) = UA\,\mathrm{d}s \tag{19}$$

which becomes

$$U'A' = UA, \tag{20}$$

when we note $\mathrm{d}s=\mathrm{d}s'\cos(\psi-\psi_0)$.

Next we note that an observer at F (Figure 17) away from the 'kink' is unaware of its presence since he observes a bulk velocity $\mathbf{w}_0$. Thus, the same number of particles must pass through the flux-tube in each configuration. The flow of particles through a flux-tube is most simply evaluated by moving with the tube, i.e., with solar-wind velocity V in the fixed frame of reference. Then (cf., Equation (16)) the bulk velocity is purely diffusive and along the magnetic-flux-tube. Equating the total flux in each configuration we obtain

$$\kappa'_{\parallel}\frac{\partial U}{\partial s'}A'\cos(\psi-\psi_0) = \kappa_{\parallel}\frac{\partial U}{\partial s}A. \tag{21}$$

Finally, using the relationship $ds = ds' \cos(\psi - \psi_0)$, and, as seems reasonable, taking situations in which the magnetic-field lines are parallel so that A and A' are each constant, we use (20) to relate U' to U in Equation (21). We obtain

$$\kappa'_{\|} = \kappa_{\|}/\cos^2(\psi - \psi_0) \tag{22}$$

as the relationship between $\kappa'_{\|}$ and $\kappa_{\|}$, which is needed in order to account for the observations.

This very simple relationship appears to be the key to the whole phenomenon of $\mathbf{w}\cdot\mathbf{e}_0 = \text{constant}$. We would like to see it established on theoretical grounds from the basic properties of magnetic fields in the interplanetary region. We would also like to see it verified by model calculations. We envisage here setting up models including moving 'kinks' with $\kappa'_{\|}$ and $\kappa_{\|}$ related by (22) and solving for a solar burst event. If our deduction (22) is correct we should find these solutions show $\mathbf{w}\cdot\mathbf{e}_0 = \text{constant}$.

4.4. The variation of decay-time constant with anisotropy

We now put forward a simple theory to account for the dependence of $1/\tau$ upon δ (or w) shown in Figure 12. It is based on sub-section (3), above, in which we showed that particles within a 'kink' and in the volume σ' at position $\mathbf{r}$, say, can be directly associated with those in a volume σ at position $\mathbf{r}-\mathbf{x}$ in a nearby section of an unperturbed flux tube. The vector $\mathbf{x}$ is the separation from σ to σ', and $\mathbf{x}$ is perpendicular to $\mathbf{e}_0$ (Figure 17).

Observations are made at a fixed point here represented by $\mathbf{r}$. Thus, writing $U_0(\mathbf{r}, t)$ for the density distribution in the unperturbed case and noting (20), we have

$$U(\mathbf{r}, t) = fU_0(\mathbf{r} - \mathbf{x}, t) \tag{23}$$

in which f represents the ratio of areas (perpendicular to $\mathbf{e}_0$) in the flux tubes containing σ and σ'. Differentiating with respect to time, and again assuming the magnetic field lines are parallel ($\partial f/\partial t = 0$), we obtain

$$\frac{1}{\tau} = -\frac{1}{U}\frac{\partial U}{\partial t} = \frac{1}{U_0}\left[-\frac{\partial U_0}{\partial t} + \frac{d\mathbf{x}}{dt}\cdot\frac{\partial U_0}{\partial \mathbf{r}}\right]_{(\mathbf{r}-\mathbf{x}, t)} \tag{24}$$

the subscript indicating that the quantities involving U_0 are to be evaluated at $(\mathbf{r}-\mathbf{x}, t)$. Since $|\mathbf{x}| \ll |\mathbf{r}|$ we replace the argument $(\mathbf{r}-\mathbf{x})$ by $\mathbf{r}$, to obtain

$$\frac{1}{\tau} = \frac{1}{\tau_0(\mathbf{r})} + \frac{d\mathbf{x}}{dt}\cdot\mathbf{G}_0(\mathbf{r}) \tag{25}$$

with $\mathbf{G}_0 = (1/U_0)\partial U_0/\partial \mathbf{r}$ the vector density gradient, and τ_0 the decay time constant under unperturbed conditions. Equation (25) indicates that the decay time is modified as the 'kink' moves past due to the distance from σ' to σ changing, i.e., under kink conditions we are seeing particles that would normally be in a different part of the interplanetary region and the time variation of this displacement causes us to observe different parts of the radial flux distribution resulting in a changed decay time.

To evaluate Equation (25) more completely we require $\mathrm{d}\mathbf{x}/\mathrm{d}t$. This is the velocity at which σ' moves away from σ, and is thus the bulk velocity additional to $\mathbf{w}_0$ required for the particles to move around the kink in the flux tube. Hence, from the previous subsection, in the late-decay phase

$$\frac{\mathrm{d}\mathbf{x}}{\mathrm{d}t} = \mathbf{w} - \mathbf{w}_0 = (\boldsymbol{\delta} - \boldsymbol{\delta}_0)\, v/3C\,. \tag{26}$$

With this result and noting that $\mathbf{G}_0$ is radial, and that $\boldsymbol{\delta}\cdot\mathbf{e}_0 = 0$, at $r = 1$ AU, Equation (25) becomes

$$\frac{1}{\tau} = \frac{1}{\tau_0(\mathbf{r})} + \frac{vG_0}{3C}(\delta - \delta_0)\sin\psi_0\,, \tag{27}$$

indicating a linear relationship between $1/\tau$ and the anisotropy amplitude δ in the late-decay phase.

Although scattered, the observational data, Figure 12, do fit a linear relationship

$$\frac{1}{\tau} = 0.049 + 5.5 \times 10^{-3}(\delta - \delta_0) \tag{28}$$

in which we have τ in hours, δ and δ_0 in percent, and $\delta_0 = 8.0\%$. These data have been discussed earlier and (28) is an alternative to (7). Identifying the coefficients of (28) obtained from the observations with those of (27) obtained from the theory, we obtain $\tau_0 = 20.5$ hr, and $G_0 = 520\mathrm{C}\%/\mathrm{AU}$ being typically $\simeq 1000\%/\mathrm{AU}$. We thus appear to have confirmation of our rather simple theory and an indirect measurement of the radial gradient in the late decay phase.

Since the gradient $\mathbf{G}_0$ produces the anisotropy $\boldsymbol{\delta}_0$, we can deduce from these known quantities the parallel diffusion coefficient. We find $\kappa_{\parallel} \approx 1.3 \times 10^{20}\ \mathrm{cm^2\ s^{-1}}$. The gradient of $\simeq 1000\%/\mathrm{AU}$ and diffusion coefficient of $1.3 \times 10^{20}\ \mathrm{cm^2\ s^{-1}}$, obtained here, compare favourably with the values of $700\%/\mathrm{AU}$ and $2.2 \times 10^{20}\ \mathrm{cm^2\ s^{-1}}$ given in Table IV, and used in subsections (1) and (2) on the energy dependence and spatial dependence of $\boldsymbol{\delta}$ in the late-decay phase.

5. Conclusions

The anisotropy vector and decay time constant for cosmic-ray protons in the kinetic energy interval $0.7 \leqslant T \leqslant 7.6$ MeV have been examined late in the solar-flare event and have been compared with concurrent interplanetary magnetic field data. The principal results are summarized below:

(1) The anisotropy late in the solar-flare event is directed from the direction $38.7° \pm$ $\pm 2.4°$ E ($\phi^*_{cr} = 321.3°$) and this direction is independent of the concurrent local magnetic-field azimuth. The azimuth of the cosmic-ray anisotropy is not generally perpendicular to the local magnetic-field vector.

(2) This invariant direction is normal to the mean magnetic field direction within the statistical error of the available data ($\sim 5°$).

(3) The amplitude of the easterly-directed cosmic-ray anisotropy is strongly dependent on the direction of the local magnetic field vector increasing from 0.5% to $\simeq 30\%$ as the magnetic azimuth changes from 360° to 250°.

(4) The decay time constant is approximately inversely proportional to the anisotropy amplitude, and thus on the azimuth of the concurrent magnetic field vector.

(5) From consideration of the present data and our previously published data it is concluded that the azimuth of the easterly anisotropy phase is invariant at 38.7 $\pm 2.4°$E over a wide range of particle speed $0.06 \leqslant \bar{\beta} \leqslant 0.56$, in contradiction to predictions of currently accepted models of solar-particle propagation.

(6) The analysis of the data confirms that, in each of the three identifiable phases of a solar flare event at these energies (i.e., early, radial, and easterly phases), the anisotropy is comprised of a radial convective component $\boldsymbol{\delta}_c$ and a diffusive component aligned with the magnetic field.

(7) The assumption that the late-time anisotropy is perpendicular to the nominal direction of Archimedes spiral everywhere in the solar cavity leads to an inconsistency with the currently accepted values of the interplanetary diffusion coefficient, viz., it requires a time decay constant of 50 hr compared with the observed value of around 20 hr.

(8) Deviations from the nominal Archimedes spiral structure have been treated as 'kinks' in the magnetic flux tubes which are convected out with the solar wind.

(9) The observations and (7) above lead us to suggest that at late times in an event, at any point $\mathbf{r}$ in the solar cavity, the bulk flow velocity of the cosmic-ray particles in the kink is such that its component in the direction of the mean magnetic field $\mathbf{e}_0$ remains constant independent of the concurrent magnetic-field direction $\mathbf{e}$, i.e.,

$$\boldsymbol{\delta} \cdot \mathbf{e}_0 = k(\mathbf{r}),$$

the constant $k(\mathbf{r})$ being a function of position $\mathbf{r}$, with value zero near Earth.

(10) Based on (9) we deduce that $\kappa'_{\parallel}$, the parallel diffusion coefficient in the 'kinked' structure, is related to $\kappa_{\parallel}$ the nominal parallel diffusion coefficient, by

$$\kappa'_{\parallel} = \kappa_{\parallel} / \cos^2(\psi - \psi_0)$$

with $\psi - \psi_0$ the angle between $\mathbf{e}$ and $\mathbf{e}_0$. This result appears to be the major theoretical deduction we make from the observations reported herein.

(11) A theory relating the decay-time-constant variation to the magnetic-field-azimuth variation from $\mathbf{e}_0$ has been derived. With this we deduce a radial gradient of 1000%/AU for the $0.7 \leqslant T \leqslant 7.6$ MeV interval and a corresponding $\kappa_{\parallel}$ of $1.3 \times \times 10^{20}$ cm^2 s^{-1}.

Acknowledgements

The cosmic-ray anisotropy data used in this analysis were obtained under National Aeronautics and Space Administration Contract NAS 5-9075. The work presented here was supported by The National Aeronautics and Space Administration Grants NGR-44-004-121, NGR-44-004-133, NGL-44-004-130, The National Science Foun-

dation Grant, GU-4020, and The National Academy of Science Grant No. 17-Day Fund. The work of L. J. Gleeson was supported under NASA Grant NGR-05-009-081.

Appendix 1

As may be seen from an examination of Figure 11, the anisotropy amplitude for periods when the magnetic field is directed into the eastern quadrants ($0<\phi_m<90°$, $180°<\phi_m<270°$) have significantly higher values than those obtained when the magnetic field is directed into the western quadrants. We present details of the selection criteria to firmly establish the validity of these data and in particular, to show that the data used in this analysis are truly interplanetary and uncontaminated by a fresh injection of particles.

In two of the events considered in this paper, viz., 16 December 1967 and 3 December 1968, the magnetic field is directed into the eastern quadrants during the eastern anisotropy phase. In Figures 2 through 5, we display the intensity time profiles and anisotropy vector diagrams for these events. The time intervals during which we detect the field aligned, radial, and eastern anisotropy, phases are indicated on these figures. In addition, we show those time intervals in which the satellite is crossing the magnetosheath.

In analyzing the experimental data from the eastern anisotropy phase during those periods in which the magnetic field is directed into the eastern quadrants ($0°<\phi_m<90$, $180<\phi_m<270$), it is essential to establish that:

(1) the magnetic field is truly interplanetary in character and

(2) no fresh injection of particles or any unusual change in the decay of the particle intensity has occurred at these times.

Examination of the magnetic-field data has established the former for both events under discussion. As indicated in Figures 2 through 5, there are three distinct intervals in these two flare events in which the magnetic field is directed into the eastern quadrants during the eastern-anisotropy phase. We now comment on each one of these time intervals.

0500–1400 UT, 8 December, 1968: A careful examination of the data for this first period reveals that the magnetic field is definitely interplanetary in character. However the intensity-time profile does show an abrupt change in the decay rate at this time. In the analysis presented in this paper, we reject the data from this period because we cannot definitely establish that it is part of the normal decay process and not due to some other process.

0200–1500 UT, 12 December, 1968: In this period, Explorer 34 is in the outer part of the magnetosheath. Explorer 35, which is definitely sampling the interplanetary field at this time, recorded a magnetic-field azimuth of $\phi_m=258°$, which is to be compared with the Explorer 34 measurement of $\phi_m=234°$. Hence it is definitely established that the interplanetary magnetic field is from the east during this time interval.

However this period was not included in the analysis because of the 24° discrepancy between the magnetic-field azimuth recorded on the satellites. By rejecting the data from this period, we immediately avoid the suspicion that this measurement was not a true representation of interplanetary conditions.

1800 UT, 20 December–1000 UT, 21 December, 1967: The magnetic field is definitely interplanetary in character and while there are several flares which could produce a fresh injection of particles, an examination of the intensity-time profile of the low energy protons at this time reveals that this possibility is extremely unlikely. Therefore we have a time interval of about 17 hr in which the cosmic-ray flux is in an eastern-anisotropy phase when the interplanetary magnetic field is also from the east. The cosmic-ray anisotropy azimuths and amplitudes corresponding to this period have been used in the present analysis.

In conclusion, it should be noted that the data rejected for the reasons given above display the same characteristics as those included in the analysis. Any conclusions drawn from our present analysis would not be radically altered by inclusion of the rejected data.

References

Allum, F. R., Palmeira, R. A. R., Rao, U. R., McCracken, K. G., Harries, J. R., and Palmer, I.: 1971, *Solar Phys.* **17**, 241.

Axford, W. I.: 1969, *Seminar on the Problem of Cosmic Ray Generation on the Sun*, Leningrad, 1969.

Bartley, W. C., McCracken, K. G., Rao, U. R., Harries, J. R., Palmeira, R. A. R., and Allum, F. R.: 1971, *Solar Phys.* **17**, 218.

Fairfield, D. H.: 1969, *J. Geophys. Res.* **74**, 3541.

Fairfield, D. H. and Ness, N. F.: 1972, *J. Geophys. Res.* **77**, 611.

Forman, M. A.: 1970a, *J. Geophys. Res.* **75**, 3147.

Forman, M. A.: 1970b, *Planetary Space Sci.* **18**, 25.

Gleeson, L. J. and Axford, W. I.: 1969, *Astrophys. Space Sci.* **2**, 431.

Innanen, W. G. and Van Allen, J. A.: 1973, *J. Geophys. Res.* **78**, 1019.

McCracken, K. G. and Rao, U. R.: 1970, *Space Sci. Rev.* **11**, 155.

McCracken, K. G., Rao, U. R., and Bukata, R. P.: 1967, *J. Geophys. Res.* **72**, 4293.

McCracken, K. G., Rao, U. R., and Ness, N. F.: 1968, *J. Geophys. Res.* **73**, 4159.

McCracken, K. G., Rao, U. R., Bukata, R. P., and Keath, E. P.: 1971, *Solar Phys.* **18**, 100.

Ness, N. F.: 1970, *Proc. XI Int. Conf. on Cosmic Rays* (Budapest), Invited Papers, p. 41.

Ng, C. K.: 1972, Ph.D. Thesis, Monash University, Victoria, Australia.

Ng. C. K., and Gleeson, L. J.: 1971a, *Proc. XII Int. Conf. on Cosmic Rays* (Hobart) **2**, 499.

Ng. C. K. and Gleeson, L. J.: 1971b, *Solar Phys.* **20**, 166.

Pyle, K. Roger: 1973, *J. Geophys. Res.* **78**, 12.

Rao, U. R., McCracken, K. G., Allum, F. R., Palmeira, R. A. R., Bartley, W. C., and Palmer, I. D.: 1971, *Solar Phys.* **19**, 209.

Rao, U. R., Allum, F. R., and McCracken, K. G.: 1973, *J. Geophys. Res.* **78**, 8409.

Roelof, E. C.: 1973, *Proc. of Calgary Conf. on Solar-Terrestrial Relations*, Calgary, August 1972, p. 411.

Wibberenz, G.: 1971, *Proc. XII Int. Conf. on Cosmic Rays* (Hobart), Rapporteur paper.

Roelof, E. C. and Krimigis, S. M.: 1973, *J. Geophys. Res.* **78**, 5375.

Wolfe, J. H.: 1972, in C. P. Sonett, P. J. Coleman and J. M. Wilcox, (eds.), *Solar Wind*, NASA-SP-308, 170.